AIRS Deconvolution and the Translation of AIRS-to-CrIS Radiances With Applications for the IR Climate Record

Howard E. Motteler, *Member, IEEE*, and L. Larrabee Strow

***Abstract*— Spectra of the earth's thermal emission as measured by the Atmospheric InfraRed Sounder (AIRS), Cross-track Infrared Sounder (CrIS), and Infrared Atmospheric Sounding Interferometer (IASI) hyperspectral sounders are becoming a significant part of the long-term climate record. These instruments have broadly similar spatial sampling, spectral resolution, and band spans. However, the spectral response functions differ in detail, leading to significant differences in observed spectra. To address this, we translate channel radiances from one sounder to another, including simulation of the response functions of the translation target. We make regular use of such translations from AIRS to CrIS and IASI to CrIS and have implemented and tested IASI-to-AIRS and CrIS-to-AIRS translations as well. Our translation from AIRS to CrIS has some novel features. AIRS is a grating spectrometer with a distinct response function for each channel, whereas CrIS is a Michaelson interferometer with a sinc response function after calibration and corrections. We use our detailed knowledge of the AIRS spectral response functions to deconvolve AIRS channel radiances to a resolution-enhanced intermediate representation. This is reconvolved to CrIS or other instrument specifications. The resulting translation is shown to be more accurate than interpolation or regression.**

***Index Terms*— Atmospheric InfraRed Sounder (AIRS), Cross-track Infrared Sounder (CrIS), deconvolution, hyperspectral, IR sounder, spectral response function.**

I. Introduction

SPECTRA of the earth's thermal emission as measured by the Atmospheric InfraRed Sounder (AIRS) [1], Cross-track Infrared Sounder (CrIS) [2], [3], and Infrared Atmospheric Sounding Interferometer (IASI) [4] hyperspectral infrared sounders are becoming a significant part of the long-term climate record. Such measurements began with AIRS in 2002 and should continue for the foreseeable future, given their important role in numerical weather prediction. These sounders are in sun-synchronous near-polar orbits, with broadly similar spatial sampling, spectral resolution, and spectral band spans. However, the spectral response functions vary in detail, and this can lead to significant differences in observed spectra.

For applications such as calibration and validation, retrievals, and the construction of a long-term climate record, we would like to work with single set of spectral response functions. This can be done by translating channel radiances from one sounder to another, including simulation of the response functions of the translation target. We make regular use of translations from AIRS to CrIS and IASI to CrIS and have implemented and tested IASI-to-AIRS and CrIS-to-AIRS translations as well. The translations from IASI include deapodization (a form of deconvolution) before reconvolution to the translation target and work very well. Ranking these translations by accuracy in comparison with calculated reference truth, we have IASI to CrIS, IASI to AIRS, AIRS to CrIS, and finally CrIS to AIRS [5]. But aside from the AIRS-to-CrIS translation, the methods used are for the most part conventional.

Our translation from AIRS to CrIS has some novel features. AIRS is a grating spectrometer with a distinct response function for each channel determined by the focal plane geometery, whereas CrIS is a Michaelson interferometer with a sinc response function after calibration and corrections. In Section II, we show how to take advantage of our detailed knowledge of the AIRS spectral response functions (SRFs) and their overlap to deconvolve channel radiances to a resolution-enhanced intermediate representation, typically a 0.1-cm^{-1} grid, the approximate resolution of the tabulated AIRS SRFs. This intermediate representation can then be reconvolved to an alternate instrument specification. Section III gives details and validation tests for an AIRS-to-CrIS translation, and Section IV for translation from AIRS to an idealized grating model. Both translations can be further improved with a statistical correction. In Section V, we consider conventional and principal component regression for an AIRS-to-CrIS translation and compare this with our deconvolution-based translation.

II. AIRS Deconvolution

The AIRS spectral response functions model channel response as a function of frequency and associate channels with nominal center frequencies. Each AIRS channel i has an associated spectral response function or SRF $\sigma_i(\upsilon)$ such that the channel radiance $c_i = \int \sigma_i(\upsilon) r(\upsilon)\, d\upsilon$, where r is

Manuscript received March 23, 2018; revised June 19, 2018; accepted August 9, 2018. Date of publication October 3, 2018; date of current version February 25, 2019. This work was supported by the NASA Earth Sciences Intercalibration Program under Grant NNX16AQ68G. *(Corresponding author: Howard E. Motteler.)*

H. E. Motteler is with the Joint Center for Earth Systems Technology, Baltimore, MD 21228 USA (e-mail: motteler@gmail.com).

L. L. Strow is with the Department of Physics, University of Maryland Baltimore County, Baltimore, MD 21250 USA (e-mail: strow@umbc.edu).

Color versions of one or more of the figures in this paper are available online at http://ieeexplore.ieee.org.

Digital Object Identifier 10.1109/TGRS.2018.2869170

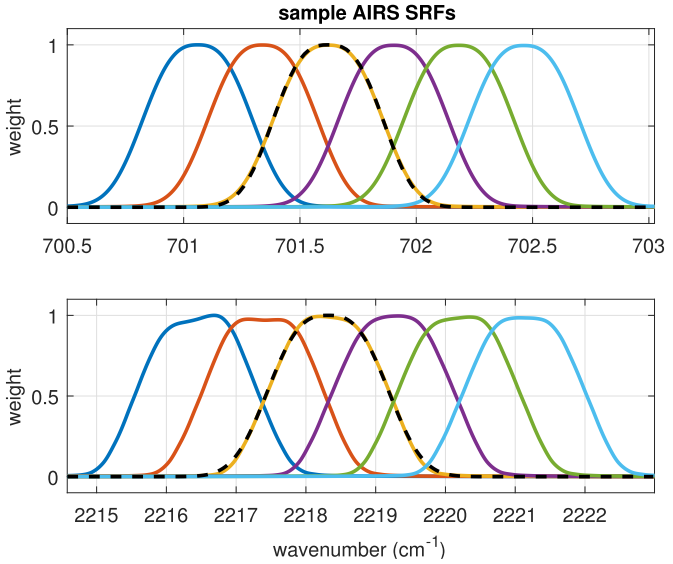

Fig. 1. Sample AIRS spectral response functions from the low and high ends of the band. Dashed line: generalized Gaussian function.

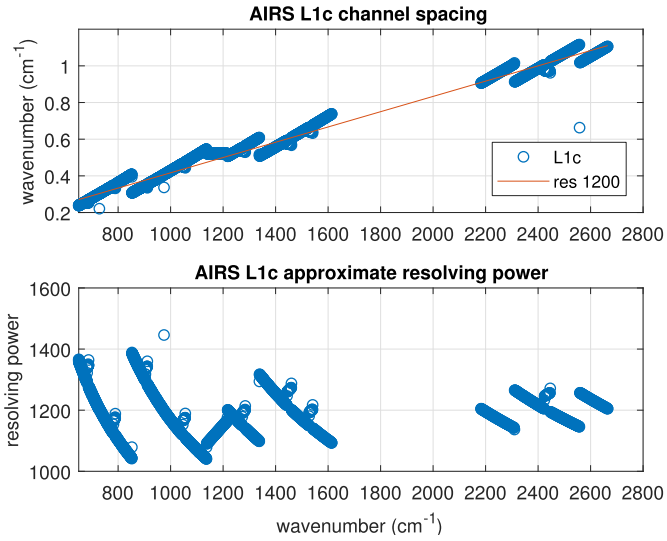

Fig. 2. AIRS L1c channel spacing and resolving power, $R = \upsilon_i/\text{FWHM}_i$. The relatively regular L1c channel spacing aids the deconvolution.

the radiance at frequency υ. The center or peak of σ_i is the nominal channel frequency.

Fig. 1 shows typical AIRS SRFs from the low and high ends of the band. Note the significant overlap in the wings. This allows the deconvolution to recover resolution beyond that of the response functions considered individually. The SRFs are not necessarily symmetrical, especially at the high end of the band, due to fringing from the AIRS entrance filters. The dashed line on the top of the third SRF in each group is a fit for a generalized Gaussian [6] of the form

$$w(\upsilon, \upsilon_0, \text{FWHM}) = \exp\left(-\left(\frac{(\upsilon-\upsilon_0)^2}{2s^2}\right)^p\right)$$

where $s = \text{FWHM}/(2\sqrt{2}\,(\ln 2)^{1/(2p)})$. Parameters υ, υ_0, and FWHM are frequency, desired channel center, and desired full-width half-max. We chose $p = 1.4$ to give an approximate match to AIRS SRFs, though without the variation or extended tails of the measured SRFs. We will use this analytic representation to calculate reference truth for the deconvolution and in Section IV as the basis for an idealized grating model.

Fig. 2 shows channel spacing and resolving power for the AIRS L1c channel set [7]. The variable channel spacing and resolving power are due to the modular structure of the focal plane. Although not entirely regular—that is, not a simple function of frequency—the L1c channel set is more regular than the L1b channel set from which it is derived, and we mainly consider the L1c set here.

Suppose we have n channels and a frequency grid $\vec{\upsilon}$ of k points spanning the union of the domains of the functions σ_i. The grid step size for our applications is often 0.0025 cm^{-1}, the default resolution for upwelling radiances calculated using the kCompressed Atmospheric Radiative Transfer Model (kCARTA) [8]. Let S_k be an $n \times k$ array such that $s_{i,j} = \sigma_i(\upsilon_j)/w_i$, where $w_i = \sum_j \sigma_i(\upsilon_j)$, that is where row i is $\sigma_i(\upsilon)$ tabulated at the grid $\vec{\upsilon}$ and normalized so the row sum is 1. If the channel centers are in increasing order, S_k is banded, and if they are not too close (as is the case for a few of the L1b channels), the rows are linearly independent. S_k is a linear transform, whose domain is radiance at the grid $\vec{\upsilon}$ and whose range is channel radiances. If r is radiance at the grid $\vec{\upsilon}$, then $c = S_k r$ gives a good approximation of the channel radiances $c_i = \int \sigma_i(\upsilon) r(\upsilon)\, d\upsilon$. In practice, this is how we calculate AIRS channel radiances for the validation tests described in the subsequent sections.

For the AIRS to CrIS and other translations, we are mainly interested in the transform S_b for SRFs at an intermediate resolution, typically 0.1 cm^{-1}. This is the approximate resolution of the SRF measurements and convenient for reconvolution to the CrIS user grid. Therefore, let $\vec{\upsilon}_b = \upsilon_1, \upsilon_2, \ldots, \upsilon_m$ be a 0.1-cm^{-1} grid spanning the domains of the functions σ_i. Similar to S_k, let S_b be an $n \times m$ array, where row i is $\sigma_i(\upsilon)$ tabulated at the $\vec{\upsilon}_b$ grid, with rows normalized to 1. If r is radiance at the $\vec{\upsilon}_b$ grid, then $c = S_b r$ is still a reasonable approximation of $\int \sigma_i(\upsilon) r(\upsilon)\, d\upsilon$.

For our application, we want to start with c and find r, that is to deconvolve c by solving $S_b r = c$ for r. Since $n < m$, the system is underdetermined. We take the Moore–Penrose pseudoinverse [9], [10] of S_b to get $r_0 = S_b^{-1} c$. This gives a minimal solution, in the sense that $||r_0||_2 \leq ||r_j||_2$ for all r_j satisfying $S_b r_j = c$. The condition number for S_b as built from the L1c channels is $||S_b||_2 ||S_b^{-1}||_2 = 115$, which is tolerable.[1]

Although our main goal is to reconvolve the deconvolved AIRS radiances to the CrIS or other user grids, as a check, we first compare the deconvolved radiances with reference truth from a direct convolution of kCARTA radiance to the 0.1-cm^{-1} grid. The response function we use for this is the generalized Gaussian above with $\text{FWHM} = \upsilon_i/2000$, where υ_i are the grid frequencies. This represents a hypothetical grating spectrometer with a resolving power of 2000, oversampled to the 0.1-cm^{-1} grid.

[1]The notation $||S||_2$ is the L^2 norm of S, which is the Euclidian distance for vectors [11].

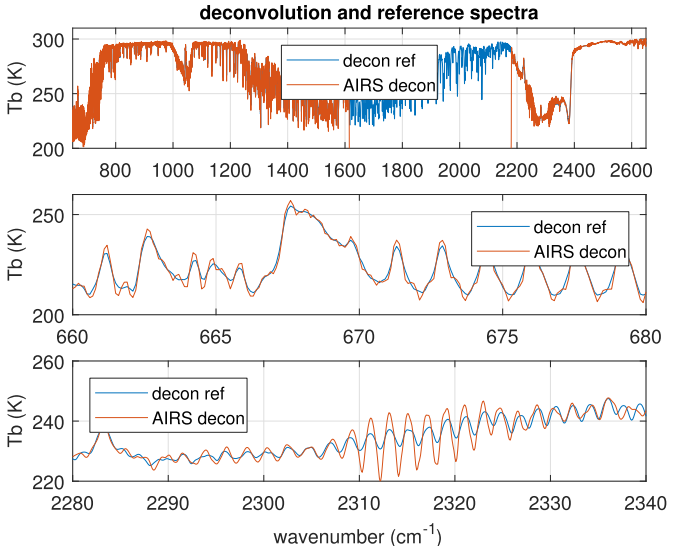

Fig. 3. Spectra from fitting profile 1 for deconvolved AIRS and the reference convolution to the 0.1-cm^{-1} grid. We see some overshoot and ringing in the deconvolution.

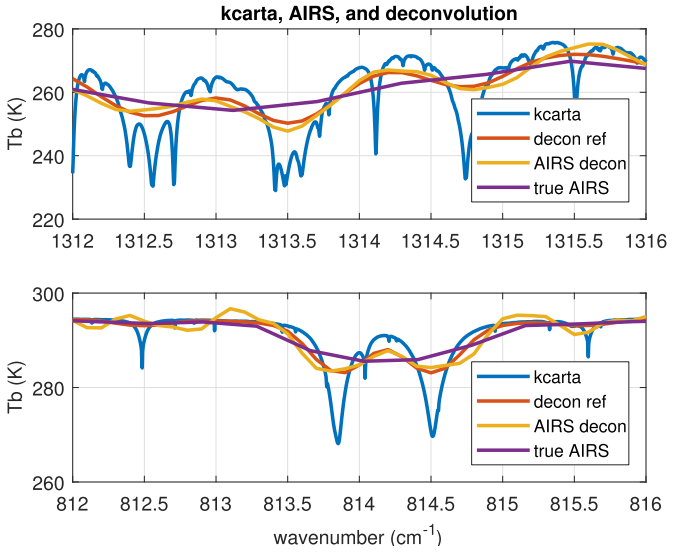

Fig. 4. Details from fitting profile 1 for kCARTA, the reference convolution to the 0.1-cm^{-1} grid, deconvolved AIRS, and true AIRS. The deconvolution restores some detail.

The AIRS deconvolution gives a modest resolution enhancement at the cost of added artifacts and noise. Fig. 3 shows spectra from fitting profile 1 [12], [13] for the AIRS deconvolution together with reference truth, with sample details from the low and high ends of the band. The ringing or overshoot at 2310 cm^{-1} is due to a change in the L1c channel spacing from 1.02 to 0.92 cm^{-1} at that point. Fig. 4 shows the details of kCARTA, the reference convolution, deconvolution, and AIRS spectra for fitting profile 1. In the first subplot, we see the deconvolution is capturing some of the fine structure in the kCARTA data that is present in the reference convolution but not the AIRS data. In the second subplot, we see the deconvolution (and reference convolution) resolving a pair of close lines that are not resolved at the AIRS L1c resolution. However, we also see some ringing that is not present in the

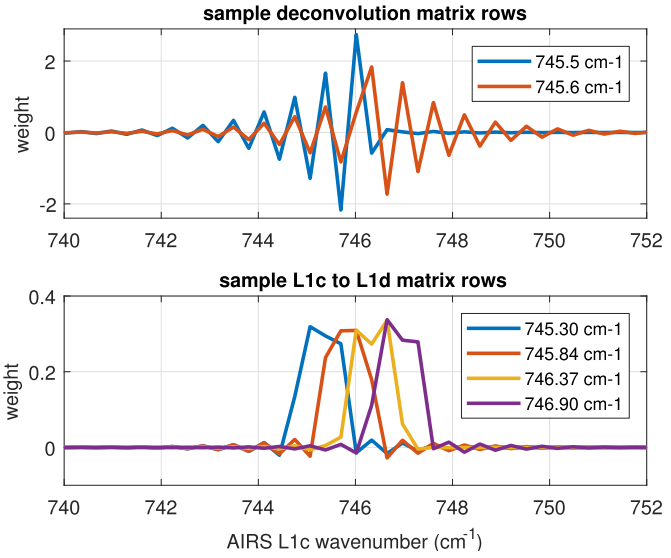

Fig. 5. Sample adjacent rows for the deconvolution and L1c-to-L1d transforms.

reference convolution. This is to be expected; significant detail is lost in the convolution to AIRS channel radiances and this can only be partially recovered by the deconvolution. The artifacts are acceptable because we do not propose using the deconvolved radiances directly; they are an intermediate step before reconvolution to a lower resolution.

Fig. 5 shows a pair of typical adjacent rows of the deconvolution matrix S_b^{-1} in the first subplot. Row i of S_b^{-1} is the weights applied to L1c channel radiances to synthesize the deconvolved radiance r_i at the intermediate grid frequency υ_i. The oscillation shows we are taking the closest AIRS channel, subtracting weighted values for channels ± 1 step away, adding weighted values for channels ± 2 steps away, and so on, with the weights decreasing quickly as we move away from υ_i, with eight to ten L1c channels making a significant contribution to each deconvolution grid point. The second subplot shows four adjacent rows of the matrix $S_d \cdot S_b^{-1}$, which takes L1c to L1d channel radiances. (The L1d radiances are discussed in the later section; here, they are of interest mainly as a typical reconvolution.) Both matrices are banded but the bands are narrower in the second, with three to five L1c channels contributing to each L1d channel. This span of influence gives us the set of parents for each translated channel.

III. AIRS-to-CrIS Translation

Given AIRS deconvolution to a 0.1-cm^{-1} intermediate grid, reconvolution to the CrIS user grid is straightforward. For CrIS standard resolution, the channel spacing is 0.625 cm^{-1} for the LW band, 1.25 cm^{-1} for the MW, and 2.5 cm^{-1} for the SW. For each CrIS band, we: 1) find the AIRS and CrIS band intersection; 2) apply a bandpass filter to the deconvolved AIRS radiances restricting them to the intersection, with a roll-off outside the passband; and 3) reconvolve the filtered spectra to the CrIS user grid with a zero-filled double Fourier transform [14]. The out-of-band roll-off smooths what would otherwise be an impulse at the band edges, reducing ringing in the translation.

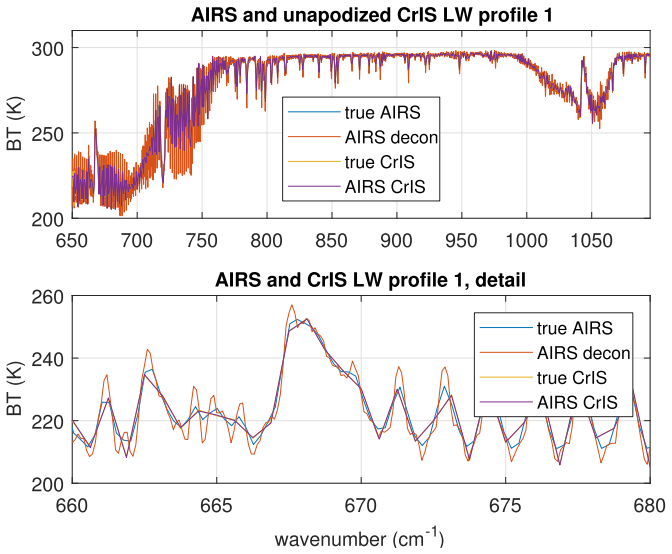

Fig. 6. True AIRS, deconvolved AIRS, true CrIS, and AIRS CrIS. Differences between true CrIS and AIRS CrIS are too small to be visible in this figure.

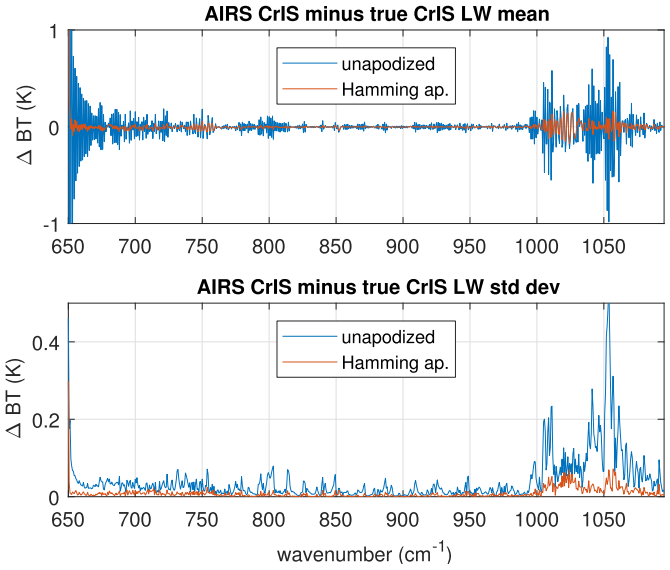

Fig. 7. Mean and standard deviation of unapodized and Hamming apodized AIRS CrIS minus true CrIS, for the LW band.

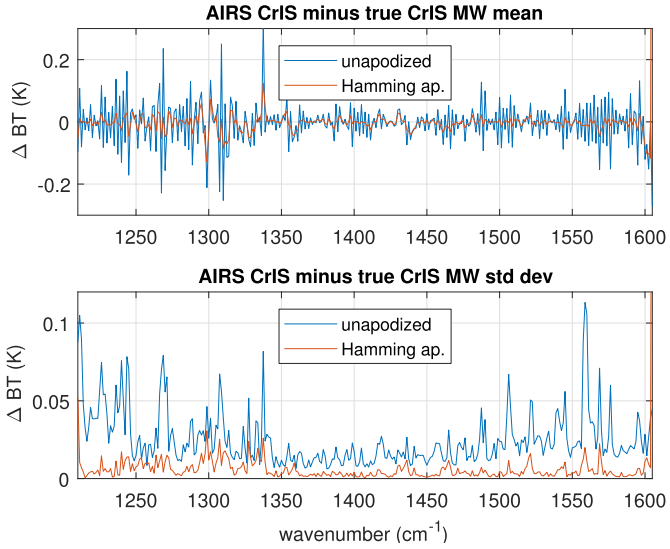

Fig. 8. Mean and standard deviation of unapodized and Hamming apodized AIRS CrIS minus true CrIS, for the MW band.

Translations are tested by comparison with calculated reference truth. We start with a set of atmospheric profiles and calculate upwelling radiance at a 0.0025-cm^{-1} grid with kCARTA [8] over a band spanning the domains of the AIRS and CrIS response functions. "True AIRS" is calculated by convolving the kCARTA radiances with AIRS SRFs and "true CrIS" by convolving kCARTA radiances to a sinc basis at the CrIS user grid. True AIRS is then translated to CrIS to get "AIRS CrIS," and this is compared with true CrIS. Fig. 6 shows sample spectra for true AIRS, deconvolved AIRS, true CrIS, and AIRS CrIS. Any difference between true CrIS and AIRS CrIS is hard to see here, and in subsequent plots, we mainly show explicit differences.

Comparisons are done both with and without apodization. Hamming apodization [15], [16] sacrifices some resolving power but gives a significant reduction in the residuals and is convenient for many applications. Convolution, deconvolution, and apodization are done with radiances, while spectra are presented and statistics are done after conversion to brightness temperatures.

We use radiance from a set of 49 fitting profiles spanning a wide range of clear atmospheric conditions as our test set, and as the independent set for statistical sets. This set was initially chosen for testing radiative transfer codes [12], [13] and is highly uncorrelated; reducing the reconstruction residual to 0.02 K requires 48 left-singular vectors. (Details of this correlation measure are given in the Appendix.) For regression tests, we use radiance from a set of 7377 all-sky (clear and cloudy) AIRS profiles spanning several consecutive days as our dependent set. This set is more correlated; reducing the reconstruction residual to 0.02 K requires 260 left-singular vectors. We did try splitting the 7377 profile set into dependent and independent subsets. Residuals for the independent set from this split were consistently smaller than from the 49-profile set, suggesting that the latter makes for a stricter test.

Figs. 7–9 show the mean and standard deviation of true CrIS minus AIRS CrIS for the 49 fitting profiles, for each CrIS band. The Hamming apodization gives a significant reduction in the residuals. Fig. 10 summarizes the results of all three bands for apodized radiances. The constant bias is very close to zero for the apodized residuals. Both the apodized and unapodized residuals are significantly less than the corresponding residuals from conventional interpolation, as shown in the Appendix.

The relatively small standard deviation of the residuals suggests some regularity, and we can see an oscillation with a period of two channel steps in several places. Up to this point, there has been no statistical component to our translation, beyond the choice of test set for validation. We feel it is important to be clear about any steps that require statistical fitting. That said, we can use a simple linear correction for a

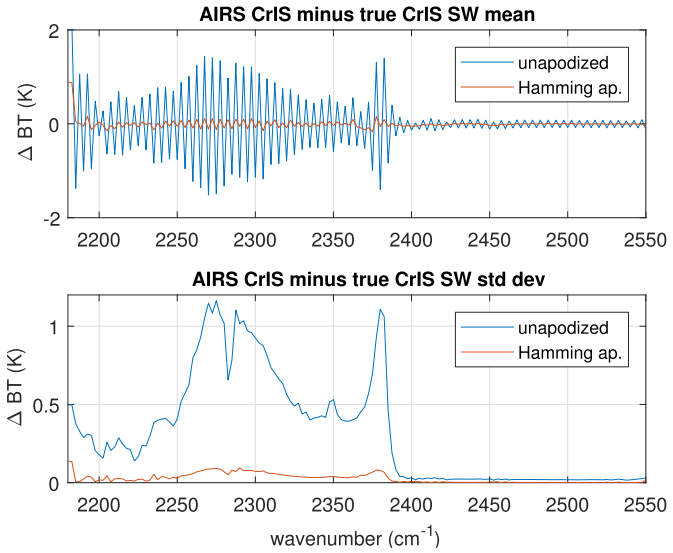

Fig. 9. Mean and standard deviation of unapodized and Hamming apodized AIRS CrIS minus true CrIS, for the SW band.

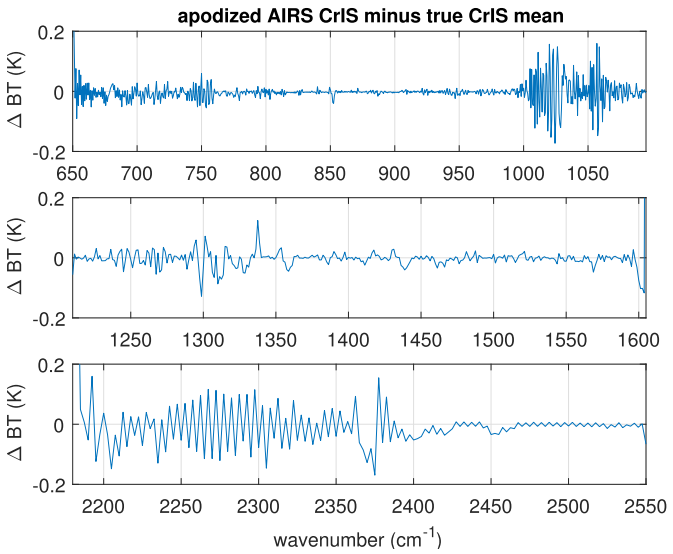

Fig. 10. Summary plot of the mean of apodized residuals for all three CrIS bands, showing the residuals in greater detail.

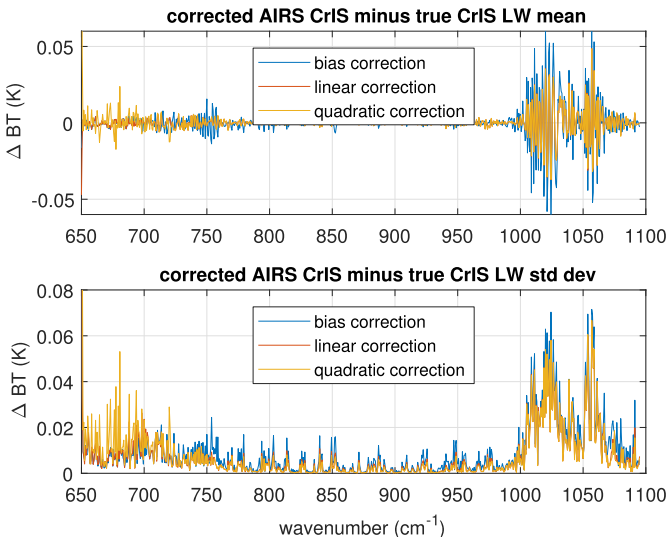

Fig. 11. Mean and standard deviation of corrected apodized AIRS CrIS minus true CrIS, for the LW band.

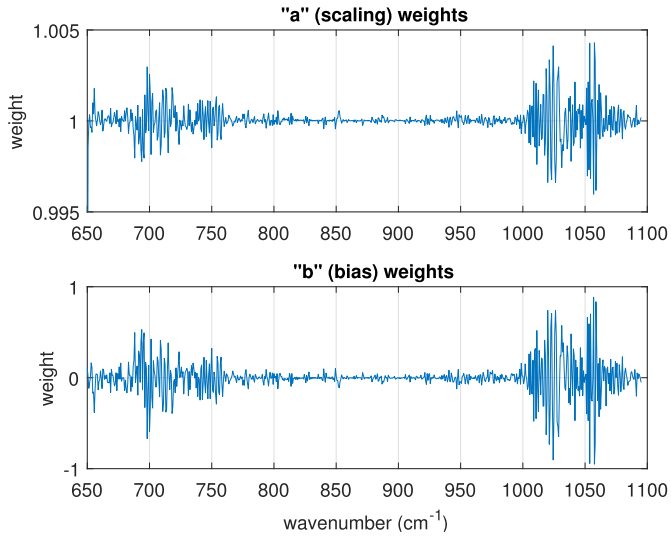

Fig. 12. Weights for the linear correction $ax + b$, for the LW band.

significant further reduction of the residuals. We use the set of 7377 mostly cloudy AIRS profiles as the dependent set and the 49 profile set as the independent or test set.

We compare three such corrections. These are done with a separate regression for each CrIS channel and so introduce no cross correlations. Let t_i^{TC} be true CrIS and t_i^{AC} AIRS CrIS brightness temperatures for CrIS channel i, from the dependent set. For the bias test, we subtract the mean residual from the dependent set. For the linear test, we find a_i and b_i to minimize $||a_i\, t_i^{\mathrm{AC}} + b_i - t_i^{\mathrm{TC}}||_2$, and for the quadratic test weights, we find c_i, a_i, and b_i to minimize $||c_i\, (t_i^{\mathrm{AC}})^2 + a_i\, t_i^{\mathrm{AC}} + b_i - t_i^{\mathrm{TC}}||_2$. The resulting correction is then applied to the independent set, the 49 fitting profiles, for comparison with true CrIS.

Fig. 11 is a comparison of bias, linear, and quadratic corrections for the LW band. The linear and quadratic corrections are nearly identical, with the quadratic coefficient very close to zero. Fig. 12 shows the weights for the linear fits from Fig. 11. The a weights are very close to 1 and the b weight to the bias. Figs. 13 and 14 show the linear correction giving a similar improvement in the MW and a small improvement in the SW, where the quadratic correction is noticably worse. Fig. 15 summarizes the residuals for the apodized linear correction for all three bands. The residuals are significantly reduced in comparison with the apodized uncorrected radiances shown in Fig. 10 and are generally less than NEdT (for the first fitting profile), as we show next.

We can give a good estimate of noise equivalent differential radiance (NEdN) for the translation by adding noise with a normal distribution at the AIRS NEdN to blackbody radiance at 280 K, translating this to CrIS, and measuring the noise of the translation. Fig. 16 shows the measured AIRS-to-CrIS NEdN together with AIRS and CrIS NEdN for both apodized and unapodized radiances. The AIRS and CrIS values are

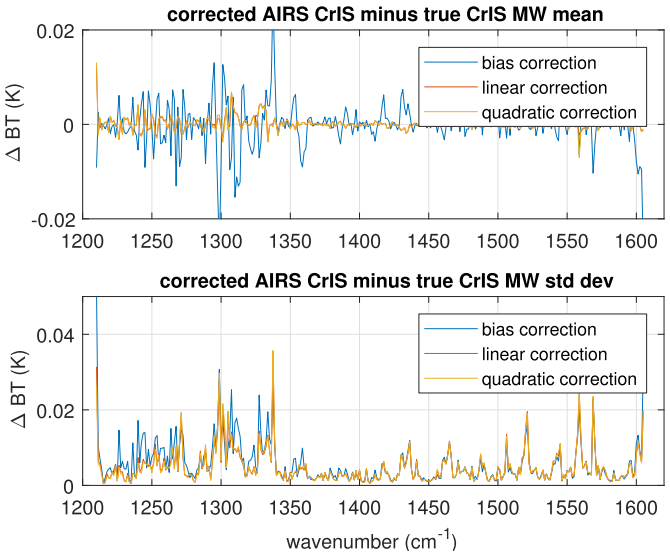

Fig. 13. Mean and standard deviation of corrected apodized AIRS CrIS minus true CrIS, for the MW band.

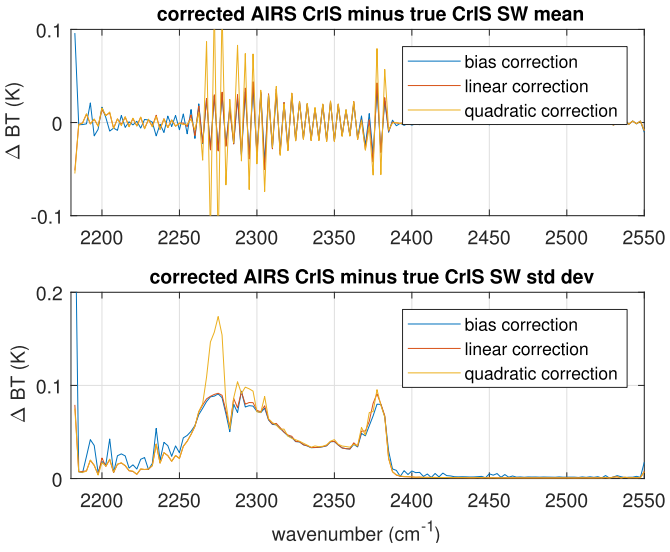

Fig. 14. Mean and standard deviation of corrected apodized AIRS CrIS minus true CrIS, for the SW band.

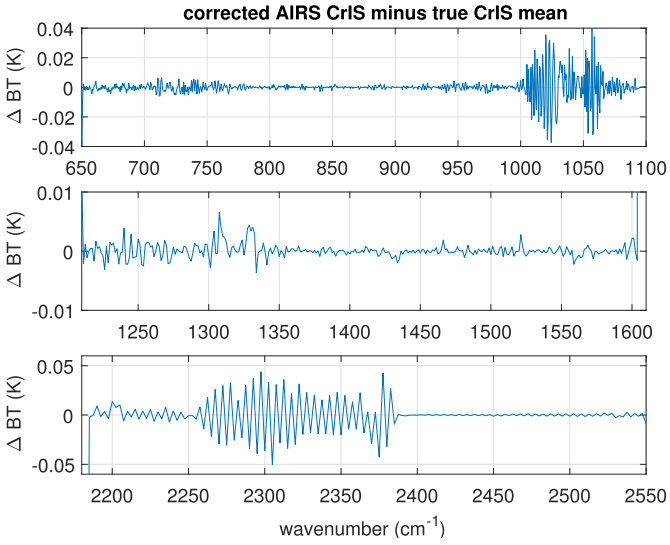

Fig. 15. Mean corrected apodized residuals for all three bands, showing the linear corrected apodized residuals in greater detail.

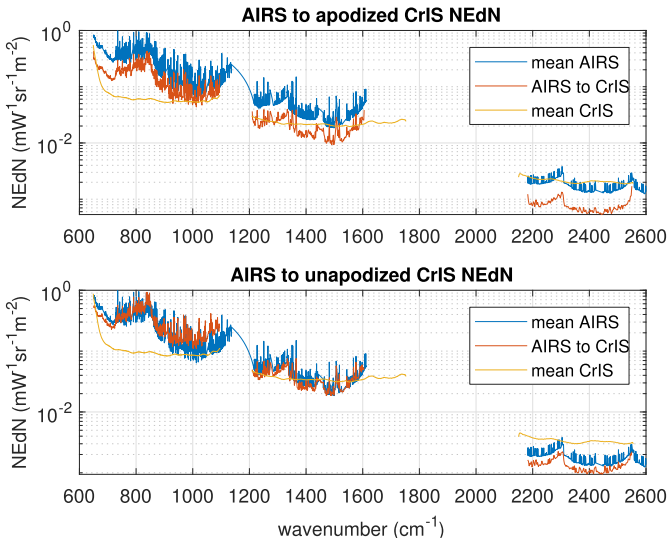

Fig. 16. AIRS, AIRS-to-CrIS, and CrIS NEdN. Apodization reduces the CrIS and AIRS-to-CrIS NEdN by a factor of 0.63.

averages over a full day, December 4, 2016. NEdN for the L1c synthetic channels is interpolated. The translation to apodized CrIS reduces NEdN significantly for all three bands. Translation to unapodized CrIS reduces NEdN slightly for the MW and SW bands, while LW NEdN is similar up to about 900 cm^{-1} and then a little higher past that. The first subplot of Fig. 17 is NEdT for apodized radiances, for fitting profile 1.

Our modeling with normally distributed noise does not consider potential correlation of the AIRS noise. The AIRS L1b data do have some noise correlation, mainly within modules. The question of correlation becomes more complex with the translation to L1c. In contrast, CrIS instrument noise is largely uncorrelated. The effect of the deconvolution-based translation is similar to a mild apodization, and so it should have a generally similar effect on the correlated component of AIRS noise. Since we are reducing NEdN in the translation (except for the LW unapodized case), it seems unlikely we are increasing problems with the correlated component, except perhaps relative to the reduced NEdN. But to prove that, we would need a plausible model of L1c noise correlation, which we do not have at the present time.

The AIRS channel-to-channel NEdN variation is significant; in the upper half of the LW and most of the MW, it is of the same order as the AIRS and CrIS NEdN difference. This variation is due to the AIRS focal plane structure and sensitivity. The AIRS and CrIS NEdN measures are both spiky when averaged over a few minutes, but the CrIS variation is primarily uncertainty in the noise measurement and smooths out as the time span is extended, while the AIRS variation is stable. The AIRS-to-CrIS translation inherits this variability; it is a significant part of the difference between AIRS CrIS and true CrIS. For a common record, we might want to add noise

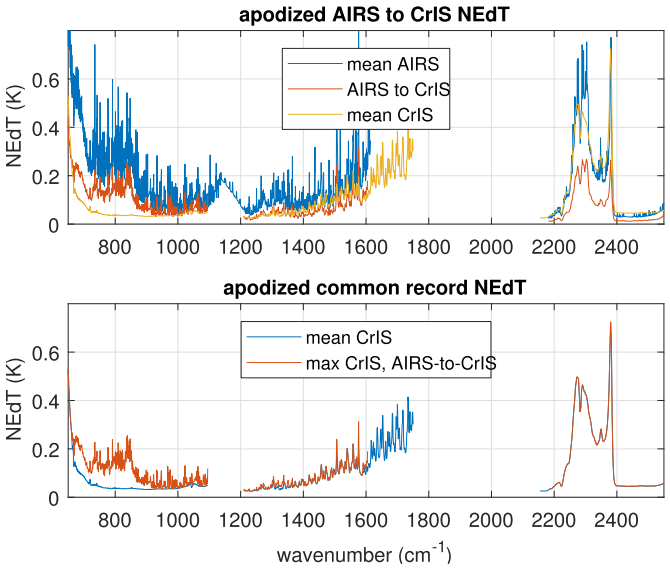

Fig. 17. AIRS, AIRS-to-CrIS, and CrIS apodized NEdT, and the max of CrIS and AIRS-to-CrIS NEdN (shown as NEdT) with CrIS NEdT shown as a reference.

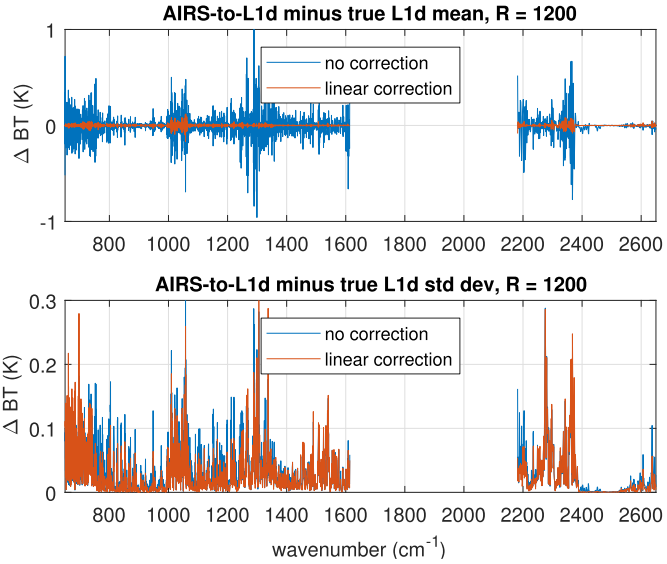

Fig. 18. Mean and standard deviation for the AIRS L1c-to-L1d translation minus true L1d, for a resolving power of 1200.

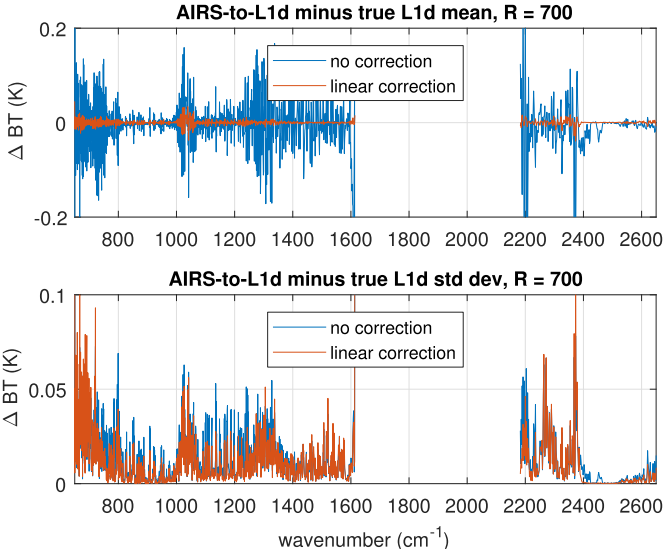

Fig. 19. Mean and standard deviation for the AIRS L1c-to-L1d translation minus true L1d, for a resolving power of 700.

on a channel-by-channel basis to whichever NEdN value—AIRS CrIS or true CrIS—is lower. NEdN for the combined record would then be max of the AIRS CrIS and true CrIS NEdN values, as shown in the second subplot of Fig. 17.

In addition to the standard resolution described above, in December 2014, CrIS switched to a high-resolution mode with a nominal OPD of 0.8 cm for all three bands, while continuing to support the standard resolution product. AIRS does not have the resolving power to properly support a translation to the CrIS high-resolution MW and SW bands—the residuals for that case are relatively large. One solution for a common record might be a compromise CrIS resolution of 0.6 cm for the MW and 0.4 cm for the SW to roughly match the AIRS resolving power. As an alternative, in Section IV, we consider translation from AIRS to an idealized grating model.

IV. Translation to an Idealized Grating Model

The AIRS deconvolution can be used for other translations. In this section, we briefly examine reconvolution to an idealized grating model for resolving powers of 700 and 1200. There are several reasons to consider such a translation. The constant resolving power of the L1d basis (defined in the following) makes it a more natural translation target for AIRS than the constant channel spacing of CrIS. It could be considered as the next step in regularization of the AIRS product, following the partial regularization from L1b to L1c, and as a potential alternative target for a long-term common record.

Define an AIRS L1d basis with resolving power R using the generalized Gaussian response function of Section II as follows. Let υ_0 be the frequency of the first channel, and for $i \geq 0$, $\text{FWHM}_i = \upsilon_i / R$, $d\upsilon_i = \text{FWHM}_i/2$, and $\upsilon_{i+1} = \upsilon_i + d\upsilon_i$. As with the tests of the AIRS-to-CrIS translation, true L1c is calculated by convolving kCARTA radiances with AIRS L1c SRFs and true L1d by convolving with an L1d basis at the desired resolving power. L1c is translated to L1d by deconvolution followed by reconvolution to the desired L1d basis, and this is compared with true L1d.

Fig. 18 shows residuals for reconvolution to an L1d basis with the resolving power of 1200, the nominal AIRS resolution, and Fig. 19 shows residuals for a resolving power of 700. Note the different x-axes for the two figures. The residuals depend in part on the L1d starting channel υ_0 and so on how the L1c and L1d SRF peaks line up. The residuals shown are the result of a rough fit for υ_0. For a resolving power of 1200, this gave υ_0 equal to the first L1c channel, while for 700, it was the first L1c channel plus 0.2 cm^{-1}.

We see that for both the AIRS-to-CrIS and L1c-to-L1d translations, some resolving power is sacrificed in shifting channel centers to a single regular function of frequency.

Residuals for a resolving power of 1200 (see Fig. 18) are roughly comparable to unapodized CrIS (see Figs. 7–9), and residuals for a resolving power of 700 (see Fig. 19) are roughly comparable to apodized CrIS (see Fig. 15). As with the AIRS-to-CrIS translation, the L1c-to-L1d residuals are significantly reduced with a linear correction. Residuals for L1d with a resolving power of 700 after correction are comparable to residuals for apodized CrIS after a similar correction.

To use the L1d basis as a common record requires translations from both AIRS and CrIS. Our focus here is primarily translations from AIRS, and details of a CrIS-to-L1d translation are beyond the scope of this paper. However, we note that the CrIS high-resolution mode allows for a CrIS-to-AIRS translation, as described in [5]. The residuals are larger in the LW than for our translation from AIRS to CrIS, but may be acceptable for some applications. The regularity and definable resolving power of the L1d basis should allow a translation from CrIS to work at least as well.

V. Direct and Principal Component Regression

We want to compare our deconvolution-based translations with other approaches to radiance translation, with an emphasis on methods we have used in the past. In this section, we consider regression-based translations, and in Section VI-B, conventional interpolation.

The AIRS L1c-to-L1d translation can be done with a single linear transform $S_d \cdot S_c^{-1}$, where S_c and S_d are the transforms taking the intermediate grid to L1c and L1d channels. The AIRS-to-CrIS translation could also be done with a composite transform if we use a resampling matrix rather than double Fourier interpolation and a matrix form of the bandpass filters. We can get such a one-step transform in other ways. Suppose r_a and r_c are $m \times k$ and $n \times k$ AIRS and CrIS radiance sets, for example true AIRS and true CrIS from Section III. We can find an $n \times m$ matrix X by regression to minimize $\|Xr_a - r_c\|_2$ and use this as our AIRS to CrIS transform. We call this standard technique "direct regression" here. This is different from the corrections of Sections III and IV; there regression was used to find linear or quadratic correction coefficients independently for each channel.

Fig. 20 shows residuals for direct regression from AIRS to apodized CrIS radiances. As before, we use the 7377 profile set as the dependent set and the 49 profile set as the independent set. The residuals are roughly comparable to the residuals from the deconvolution translation summarized in Fig. 15. However, the regression matrices show significant off-diagonal correlations. Fig. 21 shows this for the MW band; correlations are less for the LW and larger for the SW. In addition, the dependent set residuals are very small, much less than the residuals for the independent set. These are signs of overfitting. As noted in Section III, the 7377 profile dependent set is highly correlated; the effective dimension (as defined in the Appendix) is only 260.

Common techniques for reducing such correlation include adding noise, restricting the solution to a banded matrix, or working with principal component decompositions of the data. We had best results with the latter. As mentioned above, let r_a and r_c be $m \times k$ and $n \times k$ AIRS and CrIS radiance sets. Let $r_a = U_a S_a V_a^T$ be the singular value decomposition with singular values in descending order and U_a^i the first i columns of U_a. Similarly, let $r_c = U_c S_c V_c^T$ be a singular value decomposition with singular values in descending order and U_c^j the first j columns of U_c. Let $\hat{r}_a = (U_a^i)^T r_a$ and $\hat{r}_c = (U_c^j)^T r_c$ be r_a and r_c represented with respect to the bases U_a^i and U_c^j. (Since the bases are orthonormal, the transpose is the inverse.) Then, as before, find X by regression to minimize $\|X\hat{r}_a - \hat{r}_c\|_2$. This gives us $R = U_c^j X (U_a^i)^T$, an AIRS-to-CrIS transform parameterized by the basis sizes i and j.

Note that our principal component regression is not the same as regression after principal component (or singular vector) filtering; for that we would take $\bar{r}_a = U_a^i (U_a^i)^T r_a$ and $\bar{r}_c = U_c^j (U_c^j)^T r_c$, find X to minimize $\|X\bar{r}_a - \bar{r}_c\|_2$, and have no need for a change of bases to apply X. In practice, this did not work as well as doing regression after the change of bases.

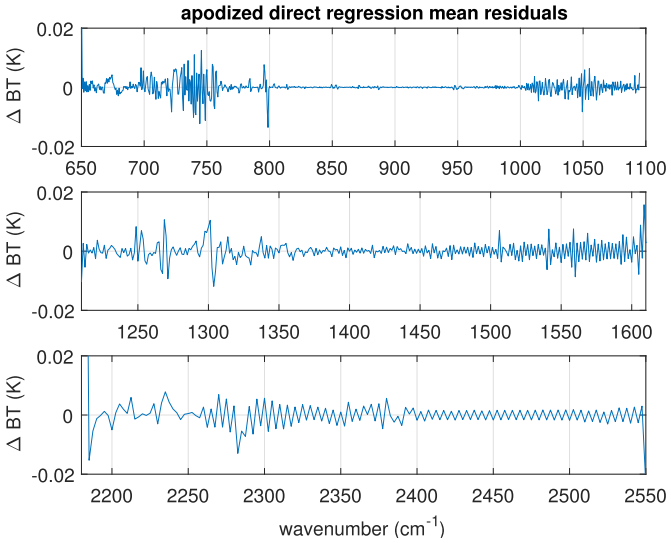

Fig. 20. Mean residuals over the 49 profile independent set for AIRS to apodized CrIS direct regression.

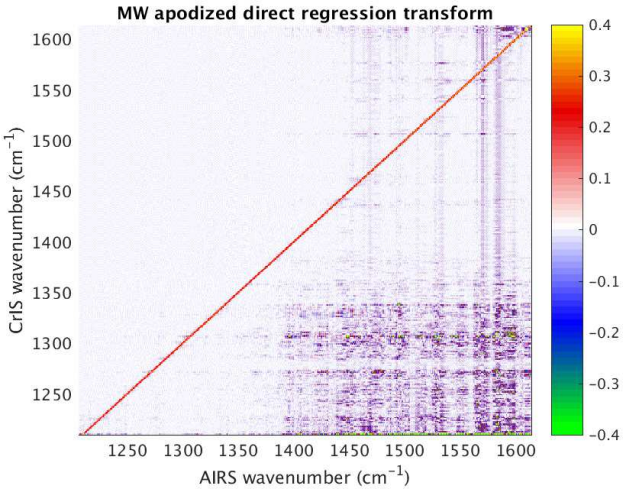

Fig. 21. Regression transform from the 7377 profile dependent set for the MW apodized direct regression transform.

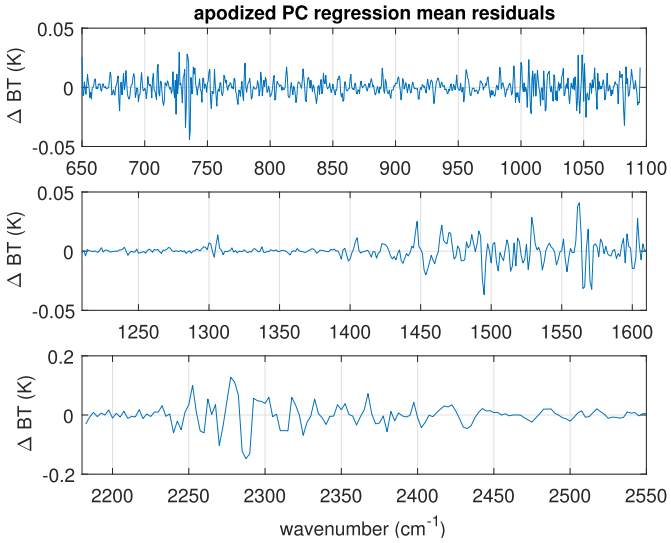

Fig. 22. Mean residuals over the 49 profile independent set for AIRS to apodized CrIS principal component regression.

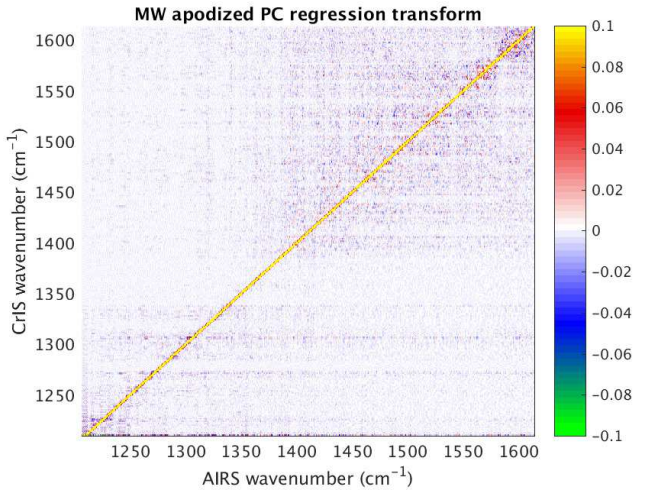

Fig. 23. Regression transform from the 7377 profile dependent set for MW apodized principal component regression with $i = 500$ and $j = 320$.

Fig. 22 shows residuals and Fig. 23 the transform R for the CrIS MW band. We have chosen $i = j = 500$ for the LW, $i = 500$ and $j = 320$ for the MW, and $i = j = 100$ for the SW for the basis sizes to roughly balance unwanted correlation with residual size. The off-diagonal correlations are significantly reduced, but the residuals are now larger than for the deconvolution-based translation summarized in Fig. 15. We conclude that principal component regression works fairly well, in comparison with regular regression or interpolation, but not quite as well as the deconvolution-based translation.

VI. Applications

We have been using the AIRS-to-CrIS and IASI-to-CrIS translations to analyze simultaneous nadir overpasses [17], [18] and hope to create a long-term climate record spanning observations from multiple sounders. The translation of response functions as discussed here is just one part of such a project. To build a common record, we must choose a target format. This might be the CrIS standard resolution, a CrIS intermediate resolution as proposed in Section III, or the generalized Gaussian basis of Section IV. The choice constrains which sounders or resolution modes can be included. For example, our proposed CrIS 0.8/0.6/0.4-cm intermediate resolution would mean dropping two and a half years (April 2012 to November 2014) of overlap of AIRS and CrIS standard resolution data. This sort of problem is inherent in building a common record—over time resolving power and band spans typically increase. However, a target format is constrained by what is available from the start.

Uniform spatial sampling is a key part of a long-term record. AIRS and CrIS sampling is similar but not identical. Details are beyond the scope of this paper, but some subsetting is typically necessary. For example, most of our sampling analysis is downstream from a "latitude weighted subset," the selection of all observations such that $X < |\cos(\text{latitude})|$, where X is a random variable from the uniform distribution $[0, 1]$ [19]. Further subsetting, to correct for sampling biases or simply to save space, may be desirable.

For some applications, these translations allow the use of a common radiative transfer model and retrieval algorithm. For applications such as assimilation and physical retrievals, the translation would need added noise, as discussed in Section III. Finally, a possible future application is to revisit the AIRS SRF measurements, to see if adjustments (within the original measurement uncertainty) can reduce the translation residuals.

Appendix

A. Measures of Correlation

We want to measure the correlation of a set of radiances. One such measure is dimension of a spanning set. For an approximation, we use the basis size needed to get reconstruction residuals below some fixed threshold. Let r_0 be an $m \times n$ array of radiances, one row per channel and one column per observation. Let $r_0 = USV^T$ be the singular value decomposition of r_0 with singular values in descending order, and U_k the first k columns of U. Let $r_k = U_k U_k^T r_0$; then $r_k \approx r_0$. The approximation improves as k increases and becomes exact for some $k <= m$. This is the analog of principal component filtering using left-singular rather than eigenvectors and is useful as a form of compression when k is small relative to m. For that case, we save U_k and $U_k^T r_0$ separately. Applications include compression of IASI radiance data and the kCARTA absorption coefficient database.

We use a threshold for equivalence that is relevant for our applications. Let B^{-1} be the inverse Planck function and define $d(r_1, r_2) = \text{rms}(B^{-1}(r_1, \upsilon) - B^{-1}(r_2, \upsilon))$, the rms difference over all channels and observations of the brightness temperatures of radiance data. Finally, let j be the smallest value such that $d(r_0, r_j) \leq T_d$, for some threshold T_d. Then, j is the effective dimension of our set r_0. Here, we have chosen $T_d = 0.02$ K. For the 49 profile fitting set, this gives $j = 48$, which we interpret as largely uncorrelated, while for the 7377 profile cloudy set, we found $j = 260$, which we interpret as highly correlated.

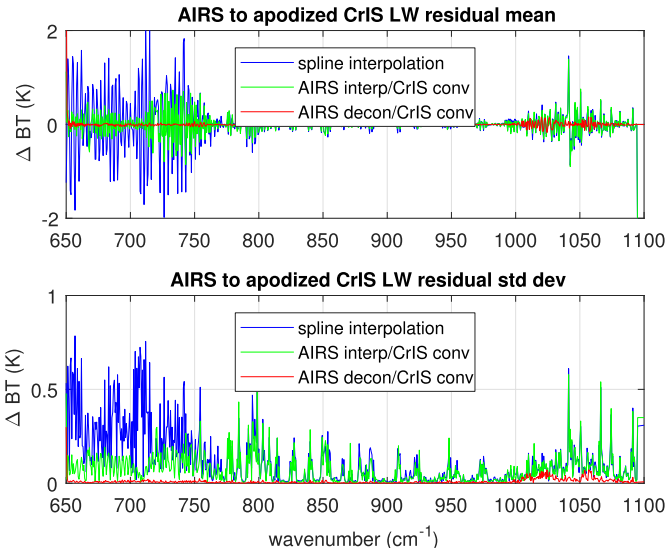

Fig. 24. AIRS to apodized CrIS translation via spline interpolation, interpolation followed by CrIS convolution, and AIRS deconvolution followed by CrIS convolution.

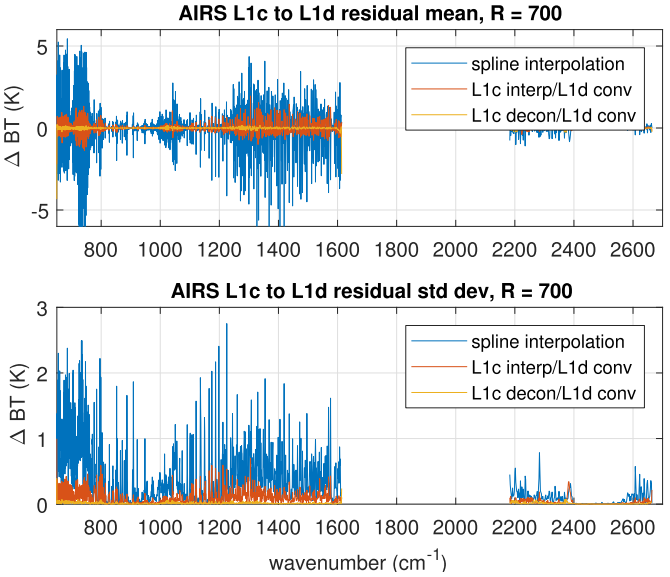

Fig. 25. AIRS L1c to L1d translation via spline interpolation, interpolation followed by L1d convolution, and L1c deconvolution followed by L1d convolution.

B. Conventional Interpolation

The AIRS-to-CrIS translation via deconvolution works significantly better than conventional interpolation. This is not surprising, since the former makes use of both the source and target response functions. We consider two cases. For the first, start with true AIRS and interpolate radiances directly to the CrIS user grid with a cubic spline. This makes no use of either the AIRS or CrIS response functions. For the second, interpolate true AIRS to the 0.1-cm^{-1} intermediate grid with a cubic spline and then convolve this to the CrIS user grid. This uses the CrIS but not the AIRS response functions. Results for apodized CrIS LW radiance are summarized in Fig. 24. As expected, residuals for spline interpolation alone are larger than that for spline interpolation followed by convolution to the CrIS user grid, and both are significantly larger than residuals for AIRS deconvolution followed by the CrIS convolution. Results for the MW and SW are similar.

The AIRS L1c-to-L1d translation via deconvolution also works significantly better than interpolation. As before, we consider two cases. For the first, start with true AIRS and interpolate radiances directly to the L1d grid with a cubic spline. For the second, interpolate true AIRS to the 0.1-cm^{-1} intermediate grid with a cubic spline and convolve this to the L1d channel set. Results for a resolving power of 700 are summarized in Fig. 25. Residuals for spline interpolation are larger than that for spline interpolation followed by convolution to the L1d channel set, and both are significantly larger than residuals for AIRS deconvolution followed by the L1d convolution.

C. Source Code

MATLAB code for the translations and tests described here (including the IASI-to-CrIS, IASI-to-AIRS, and CrIS-to-AIRS translations mentioned in the introduction) is available at GitHub: https://github.com/strow/airs_deconv and https://github.com/strow/iasi_decon.

The translations have been tested extensively. Runtime for the AIRS-to-CrIS translation is split fairly evenly between deconvolution and reconvolution. It takes about 30 s to translate our 7377 profile cloudy set running on one processor. Calculating the pseudoinverse adds another 10 s, but that only needs to be done when the translation parameters change.

REFERENCES

[1] H. H. Aumann *et al.*, "AIRS/AMSU/HSB on the Aqua mission: Design, science objectives, data products, and processing systems," *IEEE Trans. Geosci. Remote Sens.*, vol. 41, no. 2, pp. 253–264, Feb. 2003.

[2] Y. Han *et al.*, "Suomi NPP CrIS measurements, sensor data record algorithm, calibration and validation activities, and record data quality," *J. Geophys. Res., Atmos.*, vol. 118, no. 22, pp. 12734–12748, Nov. 2013.

[3] L. L. Strow *et al.*, "Spectral calibration and validation of the cross-track infrared sounder on the Suomi NPP satellite," *J. Geophys. Res., Atmos.*, vol. 118, no. 22, pp. 12486–12496, Nov. 2013.

[4] F. Hilton *et al.*, "Hyperspectral Earth observation from IASI: Five years of accomplishments," *Bull. Amer. Meteorol. Soc.*, vol. 93, pp. 347–370, Mar. 2012.

[5] H. E. Motteler and L. L. Strow. (2016). *Deconvolution and Translation Between High Spectral Resolution IR Sounders*. [Online]. Available: https://github.com/strow/airs_deconv/blob/master/doc/decon_atbd.pdf

[6] Wikipedia Contributors. *Gaussian Function*. Accessed: Nov. 12, 2017. [Online]. Available: https://en.wikipedia.org/wiki/Gaussian_function

[7] E. M. Manning, H. H. Aumann, D. A. Elliott, and L. L. Strow, "AIRS level 1C algorithm theoretical basis version 3.0," Jet Propuls. Lab., California Inst. Technol., Pasadena, CA, USA, Tech. Rep. ATBD-AIRS-L1C-01, Jan. 2015. [Online]. Available: http://eospso.gsfc.nasa.gov/sites/default/files/atbd/V6.1.0_201_AIRS_L1C_ATBD.pdf

[8] L. L. Strow, H. E. Motteler, R. G. Benson, S. E. Hannon, and S. D. Souza-Machado, "Fast computation of monochromatic infrared atmospheric transmittances using compressed look-up tables," *J. Quant. Spectrosc. Radiat. Transf.*, vol. 59, nos. 3–5, pp. 481–493, 1998. [Online]. Available: http://www.sciencedirect.com/science/article/pii/S0022407397001696

[9] Wikipedia Contributors. *Moore–Penrose Inverse*. Accessed: Nov. 12, 2017. [Online]. Available: https://en.wikipedia.org/wiki/Moore-Penrose_inverse
[10] G. Strang, *Linear Algebra and Its Applications*, 2nd ed. New York, NY, USA: Academic, 1980.
[11] Wikipedia Contributors. *Norm (Mathematics)*. Accessed: May 16, 2018. [Online]. Available: https://en.wikipedia.org/wiki/Norm_(mathematics)
[12] L. L. Strow, S. E. Hannon, S. D. Souza-Machado, H. E. Motteler, and D. Tobin, "An overview of the AIRS radiative transfer model," *IEEE Trans. Geosci. Remote Sens.*, vol. 41, no. 2, pp. 303–313, Feb. 2003.
[13] L. L. Strow, S. E. Hannon, S. D.-S. Machado, H. E. Motteler, and D. C. Tobin, "Validation of the atmospheric infrared sounder radiative transfer algorithm," *J. Geophys. Res., Atmos.*, vol. 111, no. D9, p. D09S06, 2006, doi: 10.1029/2005JD006146.
[14] H. E. Motteler and L. L. Strow. (2014). *Interferometric Interpolation*. [Online]. Available: https://github.com/strow/airs_deconv/blob/master/doc/finterp.pdf
[15] C. D. Barnet, J. M. Blaisdell, and J. Susskind, "Practical methods for rapid and accurate computation of interferometric spectra for remote sensing applications," *IEEE Trans. Geosci. Remote Sens.*, vol. 38, no. 1, pp. 169–183, Jan. 2000.
[16] Wikipedia Contributors. *Window Function*. Accessed: Nov. 12, 2017. [Online]. Available: https://en.wikipedia.org/w/index.php?title=Window_function
[17] L. Wang, Y. Han, X. Jin, Y. Chen, and D. A. Tremblay, "Radiometric consistency assessment of hyperspectral infrared sounders," *Atmos. Meas. Techn.*, vol. 8, no. 11, p. 4831, 2015.
[18] C. Hepplewhite and L. L. Strow, "A hyper-spectral multi-sensor infrared radiance data record for climate trending: Validation using simultaneous nadir observations," Tech. Rep., 2018.
[19] H. E. Motteler and L. L. Strow. (2017). *AIRS and CrIS Sampling Comparisons*. [Online]. Available: https://github.com/motteler/cris_telecon/blob/master/airs_cris_obs/airs_cris.pdf

Howard E. Motteler (M'87) received the Ph.D. degree in computer science from the University of Maryland at College Park, College Park, MD, USA, in 1987.

From 1987 to 1994, he was an Assistant Professor and from 1994 to 1998 an Associate Professor of computer science at the University of Maryland Baltimore County, Baltimore, MD, USA. From 1992 to 1993, he was an NRC Research Associate at NASA/GSFC, Greenbelt, MD, USA. Since 1998 (with a break from 2008 to 2011), he has been a Research Associate Professor at the Joint Center for Earth Systems Technology, Baltimore, MD, USA. His research interests include infrared sounder modeling and calibration and analysis of AIRS and CrIS data for validation and trending.

L. Larrabee Strow received the Ph.D. degree in physics from the University of Maryland at College Park, College Park, MD, USA, in 1981.

He is currently a Research Professor with the Department of Physics, University of Maryland Baltimore County, Baltimore, MD, USA. He is involved in remote sensing of the Earth in the infrared using high spectral resolution satellite instruments. His primary goal is to measure climate trends using infrared sensors flown by NASA, NOAA, and EUMETSAT. To that end, he is a Science Team Member of NASA's Aqua Atmospheric InfraRed Sounder (AIRS) Instrument, the NPOESS/JPSS (NOAA-20) Cross-track Infrared Sounder (CrIS), and EUMETSAT's Infrared Atmospheric Sounding Interferometer (IASI). He also provides NASA and NOAA with the radiative transfer algorithms for the retrieval of geophysical variable using AIRS, IASI, and CrIS.